Predicting lattice parameter as a function of cation disorder in $MgAl_2O_4$ spinel

2005 J. Phys.: Condens. Matter 17 7621

(http://iopscience.iop.org/0953-8984/17/48/014)

INSTITUTE OF PHYSICS PUBLISHING JOURNAL OF PHYSICS: CONDENSED MATTER

J. Phys.: Condens. Matter **17** (2005) 7621–7631 doi:10.1088/0953-8984/17/48/014

Predicting lattice parameter as a function of cation disorder in $MgAl_2O_4$ spinel

Jonathan A Ball[1], Mohsin Pirzada[1], Robin W Grimes[1], Matthew O Zacate[2], David W Price[3] and Blas P Uberuaga[4]

[1] Department of Materials, Imperial College London, SW7 2BP, UK
[2] Department of Physics and Geology, Northern Kentucky University, KY 41099, USA
[3] AWE, Aldermaston, Reading, Berkshire, RG7 4PR, UK
[4] Los Alamos National Laboratory, Los Alamos, NM 87545, USA

E-mail: r.grimes@imperial.ac.uk

Received 6 July 2005, in final form 12 October 2005
Published 11 November 2005
Online at stacks.iop.org/JPhysCM/17/7621

Abstract

In the perfect magnesium aluminate spinel structure all the tetrahedral sites are occupied by Mg^{2+} ions, while Al^{3+} ions occupy all the octahedral sites. Real $MgAl_2O_4$, however, exhibits cation disorder (inversion), so that some Mg^{2+} ions reside in octahedral sites with an equal number of Al^{3+} ions in tetrahedral sites. Atomistic simulation was used to correlate the degree of inversion with changes in lattice parameter. Results from several approaches, including a combined energy minimization–Monte Carlo technique (CEMMC), are compared with available experimental data. These show that the mean field method is not useful, while the defect volume approach can yield predictions that are useful in interpreting the CEMMC results, which agree most closely with experiment.

1. Introduction

Magnesium aluminate ($MgAl_2O_4$) spinel has demonstrated a strong resistance, under irradiation, to the formation of large defect aggregates such as dislocation loops and voids [1]. Given this resilience, the likelihood of radiation induced swelling and microcrack formation is dramatically suppressed. Consequently, $MgAl_2O_4$ has the ability to withstand neutron irradiation over a wide temperature range without degradation of its mechanical properties [2–4], whereas conversely it does amorphize under fission tracks [5]. Spinel is therefore being considered for applications which would exploit its radiation tolerance. These include use as an insulating and structural material in fusion reactors [6] and as an inert matrix target material in the nuclear transmutation of radioactive actinides [7, 8].

The ability of spinel to tolerate radiation damage is thought to be a result of two factors. The first is a high interstitial–vacancy (i–v) recombination rate [1]. The second factor is the ability

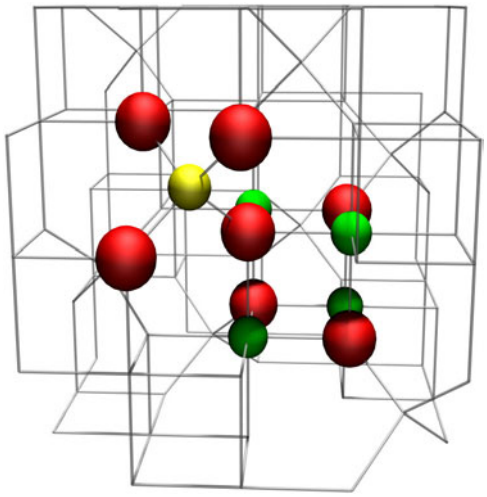

Figure 1. A single unit cell of normal $MgAl_2O_4$ spinel showing a tetrahedral Mg^{2+} coordinated by four O^{2-} ions corner linked to a cube composed of four octahedral Al^{3+} and four O^{2-} ions.
(This figure is in colour only in the electronic version)

of the lattice to tolerate significant intrinsic antisite disorder on the cation sub-lattice [9–11] as described by equation (1).

$$Mg_{Mg}^{\times} + Al_{Al}^{\times} \rightarrow Mg'_{Al} + Al^{\cdot}_{Mg}. \tag{1}$$

This is supported by neutron diffraction data from stoichiometric spinel which demonstrated significant cation disorder in a sample exposed to a high radiation dose (249 dpa at 658 K) [1]. Recent atomistic simulations of displacement cascades in spinel also resulted in high concentrations of cation antisite defects, often grouped as clusters [12]. It is, however, difficult to correlate such simulation results directly with the experimental data. One therefore needs an observable related to defect formation that can be calculated in a simulation and used to evaluate the efficacy of the method.

1.1. Inversion parameter

The extent to which the cation sub-lattice is disordered (as in equation (1)) is quantified by the inversion parameter i, the fraction of Al^{3+} cations occupying tetrahedral sites. As such, i can vary from zero, which correlates to a perfect normal spinel with all Mg^{2+} atoms on tetrahedral lattice sites, to unity, which refers to an inverse structure where all tetrahedral lattice sites are occupied by Al^{3+} ions. This is formally expressed as $(Mg_{1-i}Al_i)[Mg_iAl_{2-i}]O_4$ where parentheses refers to the tetrahedral sites and square brackets to the octahedral sites. The structure of the cation sub-lattice and the position of the cation sites with respect to the oxygen ions is displayed in figure 1.

It only requires a few minutes of equilibrating synthetic samples at high temperatures followed by quenching to induce sufficient cation exchange to raise the inversion parameter from 0.1 to values between 0.2 and 0.6 [13]. The variation of lattice parameter with respect to disorder has been shown to be small: a change in i of 0.1 modifies the lattice parameter by just 0.0025 Å [14, 15].

Natural spinel, which has been able to equilibrate over geological timescales, might be expected to have a value of i approaching zero. This is somewhat reflected in the literature,

Table 1. Short-range potential parameters.

Species	A (eV)	ρ (Å)	C (eV Å^{-6})
O^{2-}–O^{2-}	9547.92	0.2192	32.00
Al^{3+}–O^{2-}	1361.29	0.3013	—
Mg^{2+}–O^{2-}	1279.69	0.2997	—

where experimental inversion parameters vary in the range $0.025 \leqslant i \leqslant 0.12$ [16–18]. Unfortunately none of these studies reported an associated lattice parameter. Conversely the study of Hafner *et al* [19] reports the lattice parameter of natural spinel to be 8.089 ± 0.0005 Å but gave no indication as to the degree of inversion. When we compare our predictions to this lattice parameter we assume an inversion in the range 0.025–0.12.

1.2. Order–disorder in $MgAl_2O_4$

Here, atomic scale computer simulation models based on empirical potentials are shown to be capable of predicting variations in the $MgAl_2O_4$ spinel lattice parameter with cation antisite disorder (albeit with varying degrees of success). We examine disorder using a variety of analyses, including a mean-field approach, the calculation of defect volume and a novel combined energy minimization–Monte Carlo (CEMMC) technique [20, 21]. In all these cases, the simulations use energy minimization techniques and effective potentials to describe the forces between ions. The potentials were derived by fitting to room temperature structural data taken from a number of materials including MgO, Al_2O_3 and perfect $MgAl_2O_4$ (extrapolated from [14]). Consequently, we compare our results to the quenched room temperature experimental data of Andreozzi *et al* [14] and Docherty *et al* [15] on synthetic materials and the derived data described above on natural spinel [19].

2. Methodology

2.1. Pair potential simulations

The calculations presented here are based upon a classical Born-like description of an ionic crystal lattice [22, 23]. The crystal is composed of an infinite array of isotropic spherical point charges. Forces acting between ions are resolved into two terms: long-range Coulombic forces, summed using Ewald's method [24], and isotropic short-range forces, which are modelled using parametrized pair potentials. The perfect lattice is defined by a unit cell, which is effectively repeated through all space using periodic conditions.

The lattice energy, $E(r_{ij})$, can then be expressed as

$$E = \sum_{j>i}^{n} \sum_{i=1}^{n} \left[\frac{1}{4\pi\epsilon_0} \frac{q_i q_j}{r_{ij}} + A_{ij} \exp\left(\frac{-r_{ij}}{\rho_{ij}} \right) - \frac{C_{ij}}{r_{ij}^6} \right] \tag{2}$$

where A, ρ and C are parameters specific to the pair of ions i and j, r_{ij} is the interionic separation and q_i is the full formal charge of ion i. The parameters employed in this study are shown in table 1.

Defect calculations, to be used in the defect volume approach, use the Mott–Littleton methodology within which the lattice is partitioned into three concentric spherical regions, centred around the defect [25]. In region I ions are treated explicitly and relaxed iteratively to zero strain via a Newton–Raphson procedure. Region IIa is an interfacial region in which

the forces between ions are determined via the Mott–Littleton approximation [25] and ions are relaxed in one step. The interaction energies between the ions of region IIa and region I are calculated explicitly. Finally, the outer region IIb is effectively a point charge array whose relaxation energy is determined using a dielectric continuum treatment. Region IIb provides the Madelung field for the remaining crystal.

Electronic polarizability is included via the shell model for oxygen ions [26]. This assumes a massless shell with charge $-2.8|e|$ coupled to a core of charge $0.8|e|$ via an isotropic harmonic force constant 54.8 eV Å^{-2}. The net charge state of the oxygen ion is thus $-2.0|e|$. All other ions are represented by single point charges.

2.2. *Predicting lattice parameter as a function of disorder using pair potentials*

We now review the four methods employed for calculating lattice parameter as a function of defect concentration.

2.2.1. Periodic pair potential calculations. As described in section 2.1, a perfect lattice is described by identifying the ion positions within a unit cell and then repeating this through space using periodic conditions. If, in a single unit cell consisting of 56 ions, all tetrahedral sites are occupied by Mg^{2+} cations, a zero inversion ($i = 0$) perfect lattice results. If one Mg^{2+} tetrahedral cation is swapped for a near neighbour octahedral Al^{3+} cation, by virtue of the periodic conditions, we have introduced a degree of disorder into the lattice corresponding to the value $i = 0.125$. If two adjacent pairs are swapped, $i = 0.25$, and if three adjacent pairs, $i = 0.375$. The defect arrangements used for these calculations are defined in the appendix. Through energy minimization these calculations therefore provide us with four values of the spinel lattice parameter corresponding to four values of inversion parameter. Inherent in these calculations are intra-cluster defect–defect interactions, albeit specific to these cluster configurations. In addition, because of the periodic conditions, there are inter-cluster–cluster interactions.

2.2.2. Calculation of defect volumes. Local relaxations induced by defects can generate a significant expansion or contraction of the unit cell. This change in volume is specific to the type of defect and can be modelled by application of the following formula [27–29]:

$$v = -K_T V_c \left(\frac{\partial f_v}{\partial V_c}\right)_T, \tag{3}$$

where K_T (Å^3 eV^{-1}) is the isothermal compressibility, V_c (Å^3) is the unit cell volume of the perfect lattice and f_v is the internal defect formation energy calculated within the Mott–Littleton approximation.

For a cubic system, the isothermal compressibility is readily obtained from equation (4) [30],

$$K_T = [1/3(c_{11} + 2c_{12})]^{-1} \tag{4}$$

where c_{11} and c_{12} are the calculated elastic constant matrix elements. The partial derivative in equation (3) is determined numerically by conducting a series of constant volume calculations. The final unit cell volume can be established by adding the defect volumes for a given defect concentration (equivalent number of defects in a unit cell) to the perfect unit cell volume.

$$\text{Defective unit cell vol.} = \Sigma(v \times \text{number of defects per unit cell}) + V_c \tag{5}$$

where the defect volume is evaluated from equation (3). Thus, a prediction of the defect volumes generates a linear change in lattice parameter as a function of defect concentrations (inversion).

Since defect energies are calculated at the (Mott–Littleton) dilute limit a potential problem with this technique is that we completely neglect the effect of defect–defect interactions, which are likely to become increasingly important at elevated degrees of disorder. Therefore, we use the same technique, but consider the defect volume created by an adjacent pair of defects $\{Mg'_{Al}{:}Al^{\cdot}_{Mg}\}$, two pairs of defects and lastly three pairs of defects, that is, the same cluster configurations as invoked in section 2.2.1. These latter cluster cases include the effect of intra-cluster defect–defect interactions but do not include longer range inter-cluster interactions, as the defects are no longer repeated via periodic conditions.

2.2.3. Combined energy minimization—Monte Carlo (CEMMC). A comprehensive study of cation disorder in spinel is problematic; even within a single unit cell there are 735 471 possible configurations for disorder on the cation sub-lattice. Identifying and calculating the energies of each configuration would be a mammoth task. The CEMMC technique allows us to intelligently sample the possible degrees of disorder and through configurational averaging make predictions of macroscopic properties dependent upon these configurations. It has been demonstrated previously that the technique can simulate Al–Fe disorder involving uncharged defects in a study of $Ca_2Fe_xAl_{2-x}O_5$ brownmillerite over the whole compositional range $0 \leqslant x \leqslant 2.0$ [20, 21]. As is shown in the present study, the method is also successful in simulating systems containing charged defects.

Energy minimization is used to obtain the energy and lattice properties for multiple arrangements for Mg and Al within a periodically repeated supercell (i.e. not just the four arrangements in section 2.2.1) constructed from either $1 \times 1 \times 1$ or $2 \times 1 \times 1$ unit cells of stoichiometric $MgAl_2O_4$ (which contain 56 and 112 ions respectively). The arrangements are generated using the Metropolis statistical sampling Monte Carlo technique [20] as follows. At a given iteration the system has the cation configuration μ of energy E_μ. Two randomly chosen cations are then exchanged, forming a new configuration ν. The lattice is reminimized and the new energy, E_ν, is calculated and the new configuration is adopted in place of the old with probability W:

$$W_{\mu\to\nu} = \begin{cases} \exp\dfrac{-\Delta E}{kT}, & \Delta E > 0 \\ 1, & \Delta E < 0 \end{cases} \tag{6}$$

where T is the simulation's target temperature, k is Boltzmann's constant and $\Delta E = E_\nu - E_\mu$.

Within this scheme the expectation value of the quantity Q is given by

$$\langle Q \rangle = \frac{\sum_\mu Q_\mu N_\mu}{\sum_\mu N_\mu}, \tag{7}$$

where Q takes the value Q_μ for configuration μ. The value N_μ is the number of times configuration μ was chosen, either because it had been swapped into from another configuration or because it was the incumbent configuration during a failed swap attempt [20, 21].

In order to generate different overall degrees of disorder different target temperatures were employed (clearly a higher temperature gives rise to a greater overall degree of disorder). For each target temperature 6000 swap attempts (as opposed to successful swaps) are made. It was found that further increasing this number did not significantly change the inversion parameter [31].

It is stressed that contributions to the free energy of the system by lattice vibrations are included only through the quasi-harmonic approximation, for the temperature at which

potential parameters were fitted, that is room temperature. Therefore, the simulation temperatures served only to generate different degrees of average disorder and correlate to the material properties at room temperature, not at the simulation temperature. This implies that comparison should be made with experimental data derived from samples which have been quenched rapidly, thereby 'freezing in' disorder such as data from [14] (as opposed to in situ data, which would require a molecular dynamics approach such as that used recently by Lavrentiev *et al* [32]).

2.2.4. Mean field approximation. The mean field theory attempts to approximate the effect of all possible disorder by applying, between each pair of sites, a potential that is the mean of the potentials arising from all possible configurations. That is, the mean field approximation averages the potential at each lattice site with respect to the degree of disorder. While the computational ease of this method makes it desirable, it is flawed in two respects. First, it assumes all configurations are equally likely. Second, it assumes an averaged ion charge per site commensurate with the degree of disorder. The mean field analysis was conducted using the GULP code [33].

2.3. Periodic density functional calculations

In addition to pair potential simulations density functional calculations (DFT) were undertaken using the plane wave code CASTEP [34]. Due to computational restrictions calculations could only be carried out on the four configurations described in section 2.2.1, in a single unit cell, consisting of 56 ions. The system was modelled at the GGA level of approximation using the PBE functional [35] and also assuming the LDA using the CA-PZ functional [36, 37]. In both cases ultrasoft pseudopotentials were employed and a 380 eV plane wave cut-off. The Brillouin zone was sampled on a $4 \times 4 \times 4$ Monkhorst–Pack grid [38].

The aim of carrying out these quantum mechanical simulations is to provide a direct comparison to pair potential simulation (specifically those of section 2.2.1) and as such act as a further test of the potentials.

3. Results and discussions

3.1. Periodic condition simulations using DFT and pair potentials

Figure 2 compares the predicted variation in lattice parameter with increasing antisite disorder found via density functional and pair potential calculations using identical unit cell repeat units (see section 2.3). The GGA and LDA DFT calculations (square symbols and triangle symbols) overestimate the perfect spinel cell volume by 0.85% and 0.20% respectively (as can be seen from the comparison with the experimental data; crosses and star). A comparison of the DFT and pair potential techniques is nevertheless useful; both predict that the lattice parameter decreases slowly as the number of antisite pairs is increased. The GGA calculation shows a noticeably greater fall in lattice parameter between zero and one antisite pair than between subsequent points, which is not reproduced either by the LDA or by the pair potentials. It is, however, important to note that for all cases the total change in lattice parameter over the range considered is less than 0.25%.

3.2. The mean field approach

Results of the mean field analysis are presented in figure 3. Although this technique correctly predicts a negative gradient in lattice parameter as a function of inversion, the magnitude of

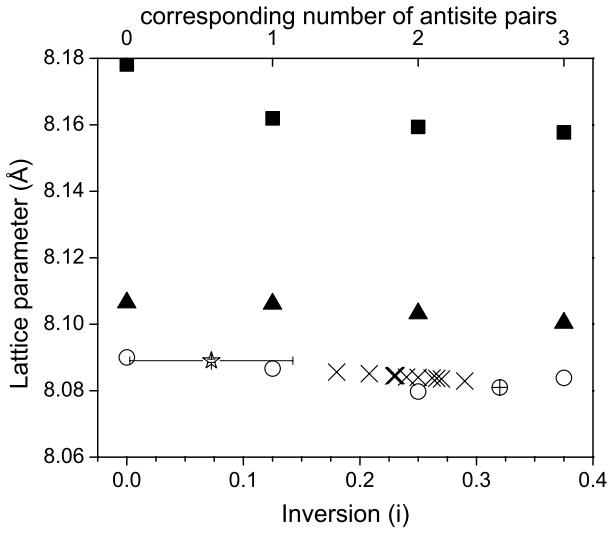

Figure 2. Variation in lattice parameter with inversion for specific defect cluster configurations containing, respectively, no, one, two and three antisite pairs. The solid square symbols correspond to GGA DFT calculations, the solid triangles to LDA DFT calculations, the open circles to pair potential calculations and the experimental data are represented as crosses [14], crossed circles [15] (synthetic samples) and a star [19] (natural sample).

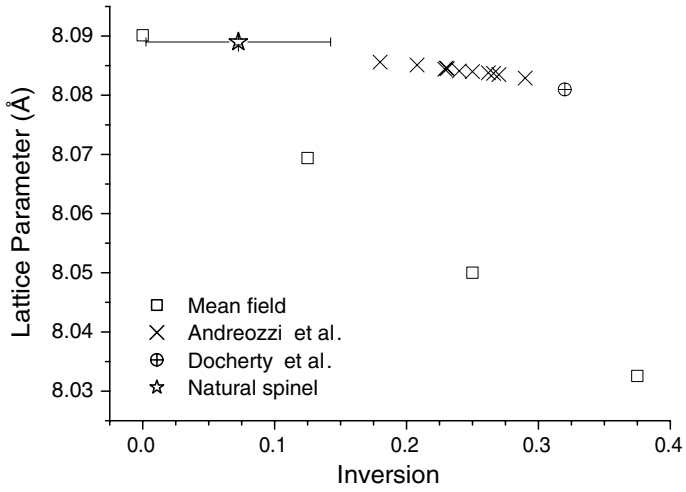

Figure 3. Variation in lattice parameter with inversion predicted using a mean field analysis. This shows significant deviation in slope from the experimental data [14, 15, 19].

this gradient is many times greater than that of the experimental data. This discrepancy is the result of overestimating the Coulomb interactions as a function of increasing disorder, which leads to lattice contraction.

3.3. Defect volume predictions

Figure 4 shows the results generated via the technique described in section 2.2.2. As it relies on multiplying the volume of a chosen defect configuration by the defect concentration, it requires

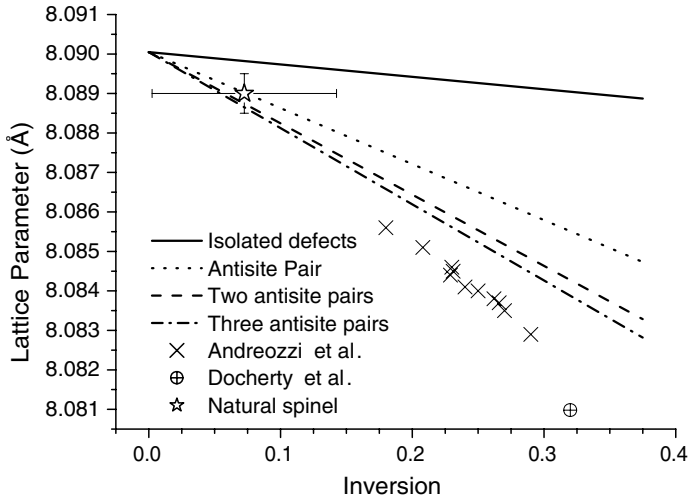

Figure 4. Variation in lattice parameter with inversion as predicted using defect volume analysis. The experimental data of Andreozzi *et al* [14], Docherty *et al* [15] and Hafner *et al* [19] are included for comparison.

Table 2. Defect volumes as predicted from equation (3).

Cluster	Volume (Å^3)
$Al^{\cdot}_{Mg}$	−0.683
Mg'_{Al}	0.606
$\{Al^{\cdot}_{Mg}:Mg'_{Al}\}$	−0.348
$2\{Al^{\cdot}_{Mg}:Mg'_{Al}\}$	−0.885
$3\{Al^{\cdot}_{Mg}:Mg'_{Al}\}$	−1.419

an *a priori* assumption as to what this defect should be. Here, results are shown assuming an isolated pair of Mg'_{Al} and $Al^{\cdot}_{Mg}$ defects, then progressively larger clusters of one, two and three nearest neighbour antisite pairs (as previously emphasized, these configurations are the same as those used for the DFT and equivalent pair potential cluster calculations). The predicted volumes are reported in table 2.

As with the other techniques, this approach is also able to reproduce the small negative gradient of the experimental data. Within these defect volume predictions a trend can be seen, in that the results become progressively closer to the experimental data on synthetic materials as the size of the cluster increases (see figure 4). Beginning with isolated defects the volumes cancel out to a significant extent (see table 2), suggesting negligible change in the lattice parameter with increasing disorder. We would, however, only expect the defects to be isolated for the very lowest values of inversion, i, when configurational entropies dominate. Conversely, the experimental data for synthetic materials correspond to a defect regime where defect–defect interactions are inevitably significant. Indeed, even the data for the natural spinel compares best to the prediction assuming cluster formation.

These results suggest that a *modestly sized* cluster can represent the majority of the effect that defect–defect interactions have on lattice parameter change. Of course, it should be noted that in this system the change in lattice parameter is rather small, thus this cluster approximation does not have to account for a great change in lattice parameter.

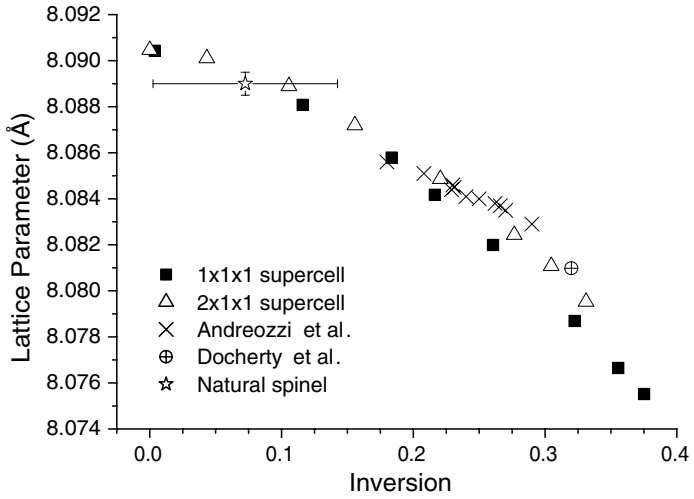

Figure 5. Variation in lattice parameter with inversion as predicted using CEMMC analysis. The experimental data of Andreozzi *et al* [14], Docherty *et al* [15] and Hafner *et al* [19] are included for comparison.

3.4. Combined energy minimization—Monte Carlo (CEMMC) predictions

In practice the lattice can be considered to contain many clusters of varying sizes in differing proportions, all of which interact. The aim of the CEMMC technique is to sample a representative distribution of defects that can reproduce the effect of such a complex system. It was found (see figure 5) that this method was able to reproduce the experimental data better than the other methods. Interestingly, the gradient of the results reproduced using the smaller supercell ($1 \times 1 \times 1$) is slightly greater than that of the experimental data for synthetic materials. Results derived using the $2 \times 1 \times 1$ supercell lie very close to these experimental results. Considering the analysis of the defect volume method, this suggests that defect–defect interactions are exaggerated by the confined $1 \times 1 \times 1$ supercell. Extension to a larger system size, such as a $2 \times 2 \times 1$ supercell, though desirable, is prohibited by the computational cost.

The CEMMC method allows us to predict the variation in lattice parameter over a wider range of inversion parameter than studied in [14, 15]. Furthermore, whereas the mean field and defect value analyses necessarily produce linear relationships for lattice parameter as a function of inversion, the CEMMC method is capable of predicting a nonlinear variation. Nonlinearity is indeed observed (figure 5), though its extent is modest. The shape of the curve predicted from the CEMMC data can be rationalized in terms of the defect volume results. At low degrees of disorder the constituent defects are likely to be in pairs (or even isolated) for entropic reasons. The variation of lattice parameter with inversion will therefore tend to follow the second line in figure 4. As defect concentrations increase, the variation will tend towards the lower two lines in figure 4. The result is a downwards curvature as observed in figure 5.

4. Summary

$MgAl_2O_4$ is usually described as having a normal spinel structure in which case all the Mg^{2+} ions should occupy all of the tetrahedral sites and the Al^{3+} ions should occupy all of the octahedral sites. In reality there is a significant and variable degree of mixing [17] between these cations. This is known as antisite disorder and for $MgAl_2O_4$ results in a modest reduction

of the lattice parameter. The degree of mixing (inversion) depends on the thermal history of the material.

Here we have described four approaches to modelling the effect of antisite disorder on the lattice parameter. These increase in statistical or computational complexity from a simple mean field method, a restricted configurational supercell approach, a calculation of defect volume applied to a consideration of defect concentration and finally a configurational averaging via a Monte Carlo simulation. In each case forces between ions were described by pair potentials, although the supercell calculations were repeated using GGA and LDA DFT methods.

The CEMMC method, which uses a Monte Carlo approach to generate defect configurations and statistically averaged lattice parameter, best reproduced the experimental data. These results suggest a slight non-linear variation in lattice parameter as a function of inversion that is not possible to discern from the experimental data. Such behaviour can be anticipated from the defect volume calculations that suggest greater variation in lattice parameter with increasing cluster formation (as would inevitably occur with greater degrees of inversion). The mean field approach that assumes an average distribution of Al^{3+} and Mg^{2+} ions commensurate with a given inversion is shown to yield much less satisfactory results.

In conclusion, the results demonstrate that a statistically derived distribution of charged antisite defects can reproduce the experimentally observed variation in lattice parameter. A method based on pair potentials is thus able to model certain residual defects in $MgAl_2O_4$ that are formed as a consequence of radiation damage. It does not, of course, establish that the methodology is able to model the dynamical processes whereby the defects are formed. As a step towards this, we will subsequently model ion migration in this system.

Acknowledgments

This work was supported by the United States Department of Energy, Office of Science, Office of Basic Energy Sciences, Division of Materials Sciences. JAB was supported by AWE and EPSRC. This work was carried out as part of the UKERC materials programme. Comments and suggestions from Kurt Sickafus, Art Voter, Roger Smith and Michael Ruston are gratefully acknowledged.

Appendix. Defect positions within a single unit cell

If the $MgAl_2O_4$ spinel structure is described using the space group $Fd3m$, in the normal (defect free) lattice Mg^{2+} and Al^{3+} cations occupy 8a and 16d Wyckoff positions respectively (see table A.1).

Table A.1. Perfect lattice positions in normal $MgAl_2O_4$.

Species	Wyckoff position	Fractional coordinates
Mg	8a	0,0,0; 1/4, 1/4, 1/4; F.C.
Al	16d	5/8, 5/8, 5/8; 5/8, 7/8, 7/8; 7/8, 5/8, 7/8; 7/8, 7/8, 5/8; F.C.

Table A.2. Defect coordinates for arrangements of two and three antisite pairs.

Configuration	Wyckoff position	Defect species	Defect coordinates
$2\{Al^{\cdot}_{Mg}{:}Mg'_{Al}\}$	$Al^{\cdot}_{Mg}$	8a	1/4, 1/4, 1/4; 3/4, 1/4, 3/4
	$Mg^{\cdot}_{Al}$	16d	5/8, 1/8, 1/8; 3/8, 1/8, 7/8
$3\{Al^{\cdot}_{Mg}{:}Mg'_{Al}\}$	$Al^{\cdot}_{Mg}$	8a	0, 1/2, 1/2; 1/2, 0, 1/2; 1/2, 1/2, 0
	$Mg^{\cdot}_{Al}$	16d	5/8, 1/8, 1/8; 1/8, 5/8, 1/8; 1/8, 1/8, 5/8

There is only one distinct way of arranging a nearest neighbour antisite cluster. For the larger clusters of two and three nearest neighbour antisite pairs the defects can be placed in multiple distinct arrangements. The defect coordinates used in this study are listed in table A.2.

References

[1] Sickafus K E, Larson A C, Yu N and Nastasi M 1995 *J. Nucl. Mater.* **219** 128
[2] Buckley S N and Shaibani S J 1987 *Phil. Mag. Lett.* **55** 15
[3] Buckley S N 1986 *J. Nucl. Mater.* **143** 387
[4] Kinoshita C and Nakai K 1989 *Japan–France Seminar Series 2: (Lattice Defects in Ceramics, Tokyo)*
[5] Sickafus *et al* 1999 *Am. Ceram. Soc. Bull.* **78** 69
[6] Skvortsova V, Mironova-Ulmane N and Ulmanis U 2002 *Nucl. Instrum. Methods Phys. Res.* **191** 256
[7] Matzke H, Rondinella V V and Wiss T 1999 *J. Nucl. Mater.* **274** 47
[8] Chauvin N, Konigs R J M and Matzke H 1999 *J. Nucl. Mater.* **274** 105
[9] Cooper E A, Hughes C D, Earl W L and Sickafus K E 1995 *Mater. Res. Soc. Symp. Proc.* **373** 413
[10] Spence J C H and Taft J 1983 *J. Microsc.* **130** 147
[11] Soeda T, Matsumura S, Kinoshita C and Zaluzec N L 2000 *J. Nucl. Mater.* **283** 952
[12] Smith R, Bacorisen D, Uberuaga B P, Sickafus K E, Ball J A and Grimes R W 2005 *J. Phys.: Condens. Matter* **17** 875
[13] Baumgartner O, Preisinger A, Heger G and Guth H 1981 *Acta Crystallogr.* A **37** C187
[14] Andreozzi G B, Princivalle F, Skogby H and Giusta A D 2000 *Am. Miner.* **85** 1164
[15] Docherty F T *et al* 2001 *Ultramicroscopy* **86** 273
[16] Schmocker U *et al* 1972 *Phys. Lett.* **40A** 237
[17] Schmocker U and Waldner F 1976 *J. Phys. C: Solid State Phys.* **9** L235
[18] Gobbi G C *et al* 1985 *Chem. Lett.* **6** 771
[19] Hafner S and Laves F 1961 *Z. Kristallogr.* **115** 331
[20] Zacate M O and Grimes R W 2000 *Phil. Mag.* A **80** 797
[21] Zacate M O and Grimes R W 2002 *J. Phys. Chem. Solids* **63** 675
[22] Born M and Mayer J 1932 *Z. Phys.* **75** 1
[23] Born M and Mayer J 1933 *J. Chem. Phys.* **1** 270
[24] Ewald P P 1921 *Ann. Phys.* **64** 253
[25] Mott N F and Littleton M J 1938 *Trans. Faraday. Soc.* **34** 485
[26] Dick B G and Overhauser A W 1958 *Phys. Rev.* **112** 90
[27] Catlow C R A, Corish J, Jacobs P W M and Lidiard A B 1981 *J. Phys. C: Solid State Phys.* **14** 121
[28] Vyas S, Grimes R W, Binks J D and Rey F 1997 *J. Phys. Chem. Solids* **58** 1619
[29] Stoneham A M 1983 *J. Phys. C: Solid State Phys.* **16** L925
[30] Nye J F 1985 *Physical Properties of Crystals* (Oxford: Oxford University Press)
[31] Pirzada M 2003 Atomic scale computer simulations of pyrochlore and spinel oxides *PhD Thesis* Imperial College, London
[32] Lavrentiev M Y, Purton J A and Allan N L 2003 *Am. Miner.* **88** 1522
[33] Gale J D 1997 *J. Chem. Soc. Faraday Trans.* **93** 629
[34] Segall M D, Lindan P J D, Probert M J, Pickard C J, Hasnip P J, Clark S J and Payne M C 2002 *J. Phys.: Condens. Matter* **14** 2717
[35] Perdew J P, Burke K and Ernzerhof M 1996 *Phys. Rev. Lett.* **77** 3865
[36] Ceperley D M and Alder B J 1980 *Phys. Rev. Lett.* **45** 566
[37] Perdew J P and Zunger A 1981 *Phys. Rev.* B **23** 5048
[38] Monkhorst H J and Pack J D 1976 *Phys. Rev.* B **13** 5188